Materials Characterization 153 (2019) 240–250

Contents lists available at ScienceDirect

Materials Characterization

journal homepage: www.elsevier.com/locate/matchar

Microstructure evolution of Al6061 and copper during ultrasonic energy assisted compression

Anagh Deshpande, Alireza Tofangchi, Keng Hsu*

J. B. Speed School of Engineering, University of Louisville, United States of America

ABSTRACT

Metal forming is often performed at elevated temperatures, typically above the recrystallization temperature of metals, which results in a reduction in yield stress during forming. Similar reduction in yield stress can also be achieved by simultaneous application of ultrasonic energy during deformation. The resulting softening of metals causes a reduction in the forming forces and increased ductility. A thorough understanding of the effect of ultrasonic energy irradiation during deformation on the microstructure is lacking which seems to be inhibiting wider adoption of ultrasonic energy in more manufacturing processes. In this manuscript, a detailed analysis of the microstructure of aluminum 6061 alloy and copper, which have identical Faced-Center Cubic crystal structure but different stacking fault energies, has been presented. Focus has been placed on the differences between their microstructure evolution behaviors after deformation under simultaneous application of ultrasonic energy. These differences have been distinctly highlighted using Electron Backscatter Diffraction (EBSD) and TEM analysis. EBSD analysis revealed assistance to subgrain formation due to ultrasonic energy. It was also observed that due to lack of dynamic recovery, copper underwent discontinuous dynamic recrystallization (DDRX) during ultrasonic energy assisted deformation. On the other hand, the recrystallization mechanism in Al6061 alloy was found to be geometric dynamic recrystallization (gDRX). The insights obtained in this work potentially advance the understanding of mechanisms governing microstructure evolution during ultrasonic energy assisted deformation and establish analogy between the mechanisms governing thermomechanical processing and ultrasonic energy assisted deformation.

1. Introduction

Thermomechanical processing is extensively used for metal shaping. The reduction in yield stress due to elevated temperature processing reduces the forces required for shaping or forming. It was observed in the 1960s that, similar to deformation at elevated temperature, deformation under the simultaneous application of high frequency acoustic energy (or ultrasonic energy) also results in a reduction in yield stress of metals [1]. This phenomenon is called acoustic/ultrasonic softening. Ultrasonic softening has three distinct characteristics. First, it is a transient phenomenon which ceases to exist once the ultrasonic energy irradiation is stopped. This could potentially help to eliminate cooling time or quenching operations after material processing. The second characteristic is that the amount of ultrasonic energy required to achieve equivalent softening is orders of magnitude lesser than the amount of thermal energy [1]. The third characteristic is that effect of ultrasonic energy can be localized. These unique characteristics present a potential for the use of ultrasonic energy during metal shaping as an alternative to thermomechanical processing.

Ultrasonic energy has been incorporated in wire drawing by Yang et al. [2], in forming by Amini et al. [3] and Abdullah et al. [4], and in friction stir welding by Zhong et al. [5], to take advantage of one or more of the characteristics of ultrasonic softening outlined above. As another example, wire bonding is a process that is routinely used in the semiconductor industry to achieve electrical connection between two pads in an integrated circuit (IC) or a semiconductor device. During this process, ultrasonic energy is used to simultaneously deform and bond metal wires onto bond pads. Ultrasonic energy softens the metal wires, thereby enabling their plastic deformation on the bond pad at stresses much lower than the yield stress of metals. Simultaneously, the wire also bonds to the bond pad establishing an electrical connection [6–8]. More recently, ultrasonic energy has been used in hybrid additive manufacturing process called Ultrasonic Consolidation [9–11] and also in ultrasonic welding [12–15]. In our previous work, a new ultrasonic energy based solid-state additive manufacturing process was demonstrated that uses wires as starting material to fabricate near net-shape components in ambient condition [16]. Despite some of its advantages, one main roadblock in the adoption of ultrasonic energy in manufacturing processes has been the lack of understanding of the ultrasonic softening phenomenon.

Since the first observation of the ultrasonic softening phenomenon, the effect of ultrasonic energy on the flow stresses during plastic deformation has been investigated and attempts have been made by several researchers to model the behavior [17–19]. The main focus of most of the investigations has been aluminum or aluminum alloys. Nevertheless, the fundamental understanding of the physics of the

* Corresponding author.
E-mail address: keng.h.hsu@gmail.com (K. Hsu).

https://doi.org/10.1016/j.matchar.2019.05.005
Received 29 January 2019; Received in revised form 16 April 2019; Accepted 3 May 2019
Available online 04 May 2019
1044-5803/

softening phenomenon is still incomplete, especially with regards to its effects on the microstructure evolution during deformation process. The insight towards microstructure evolution is critical since the post-deformation microstructure determines the final mechanical properties of the deformed metal. Some efforts have been made to this end by researchers. In the context of ultrasonic welding or ultrasonic consolidation, the focus in the literature has been on analyzing the microstructure at the interfaces between the welded materials [9,14]. In such studies, it becomes difficult to decouple the impact of frictional heating and ultrasonic energy on the microstructure evolution. In other studies that have analyzed the bulk microstructure, it has been observed that the microstructure before and after welding (or consolidation) did not significantly alter because of the very low strain experienced by the bulk of the foil [20]. Siddiq and El Sayed used a crystal plasticity model to predict the microstructure in ultrasonic consolidation of pure aluminum. The model predicts formation of subgrains at a strain of about 0.1 [21]. The same crystal plasticity FEM model was also used to predict subgrain formation in aluminum after ultrasonic energy assisted deformation [22]. Zhou et al. used Electron Backscatter Diffraction Analysis (EBSD) to compare the post-deformation microstructure of aluminum and titanium after ultrasonic-assisted compression [23]. Siu et al. used EBSD and TEM analysis to investigate the microstructure and dislocation substructure of aluminum after ultrasonic energy assisted indentation, and dislocation dynamic simulation was used to hypothesize that ultrasonic energy provides a superimposed oscillatory stress which facilitates dislocation annihilation. Similar annihilation of dislocations during ultrasonic energy assisted deformation, which led to coarsening of the subgrain network, was observed in our previous study as well [24]. The cause of this annihilation remains to be verified. The enhanced dislocation annihilation was taken into account to model the stress evolution during deformation. The summary of results regarding ultrasonic assisted deformation of 300 μm aluminum wire has been given in Fig. 1 [24].

In the following work described in this manuscript, the effect of stacking fault energy on the microstructure evolution during ultrasonic energy assisted compression has been investigated using EBSD and TEM analysis of aluminum, copper and aluminum 6061 alloy. An analogy between the resulting microstructure after hot deformation and ultrasonic assisted deformation has been shown. A detailed analysis through comparison between high stacking fault energy material (aluminum) and medium stacking fault energy material (copper) has been presented.

The effect of stacking fault energy on microstructure evolution during hot working of metals is well understood. For FCC metals, the motion of dislocations in the (111) closed packed slip plane happens along the ⟨110⟩ direction. Whether the motion of dislocations happens as perfect dislocations or through dissociation of dislocations into 2 partial dislocations (Shockley partial dislocations) is determined by the stacking fault energy of the material. For metals such as gold, nickel and copper with low to medium stacking fault energy, the motion of dislocation by dissociation into 2 partials is favored since the energy required to generate the wide stacking fault associated with dissociation is lesser. The dissociation and formation of this stacking fault inhibits climb and cross-slip which restricts recovery and results in an increase in dislocation density. Beyond a certain limit, the local difference in dislocation density results in grain nucleation. This phenomenon of new grain nucleation and growth during deformation is called discontinuous dynamic recrystallization (DDRX). For high stacking fault energy materials like aluminum, the dissociation of dislocations is not energetically favored. Hence the motion of dislocations happens as perfect dislocations or with a stacking fault with a very small width. This promotes climb and cross-slip, facilitating dynamic recovery (DRV). The resulting microstructure in the high stacking fault energy materials contains subgrains with grain-interiors having much lower dislocation densities [25,26]. However, aluminum and aluminum alloys have been shown to exhibit recrystallization behavior during hot deformation. This unique recrystallization behavior is caused by formation of serrated grain boundaries due to subgrains and subsequent pinching-off of these serrated grain boundaries at a high enough strain which results in formation of new grains. This type of recrystallization is called geometric dynamic recrystallization (gDRX) [25–27].

A similar fundamental understanding and analysis for post-deformation microstructure of metals deformed under the influence of ultrasonic energy is crucial for the wide spread-application and use of ultrasonic energy in manufacturing processes. The work presented in this manuscript provides detailed insights into the effect of ultrasonic energy on microstructure evolution of FCC metals with different stacking fault energies.

2. Experimental methods

2.1. Apparatus

The experimental apparatus for compression testing of 200 μm metal filaments (or wires) is shown in Fig. 2. The apparatus consists of an ultrasonic energy coupling tool that is connected to a piezo-electric crystal through a stainless-steel horn. The resonant frequency of the system is designed to be 40 kHz. A metal filament is fed under the ultrasonic energy coupling tool. The tool compresses the filament at a predefined strain rate. For all the experiments performed, a constant strain rate of 6 s^{-1} was used. The amount of ultrasonic energy density applied to the metal filament during compression was controlled by varying the amplitude of vibration of the ultrasonic energy coupling tool. The ultrasonic energy density was calculated using the formula, $E = a^2\omega^2\rho$, where a is the vibration amplitude measured at the tip of the ultrasonic energy coupling tool using a vibrometer in m, ω is the vibration frequency in rad/s and ρ is the density of the filament being deformed in kg/m^3. The assumption here is that all the ultrasonic vibration at the tool tip is transmitted to the filament being deformed.

2.2. Sample preparation for microstructural analysis

Copper and Al6061 filaments were deformed under the application of two different ultrasonic energy densities (500 J/m^3 and 710 J/m^3 for copper and 150 J/m^3 and 215 J/m^3 for Al6061). A cross section of the deformed filaments was cut, and standard polishing sequence was followed to prepare the samples for EBSD analysis. The samples were initially embedded in a two-part epoxy resin for convenience during polishing. Beginning with a 320 grit SiC abrasive paper, the samples were mechanically polished by abrasive papers with progressively increasing grit up to 1200 grit. This was followed by polishing with 3 μm polycrystalline diamond slurry, 0.5 μm polycrystalline diamond slurry and 0.05 μm colloidal silica slurry. The final polishing step was to polish the samples in a vibratory polisher for 4–5 h using 0.05 μm colloidal silica slurry. Samples were cleaned in an ultrasonic bath between each polishing step. These samples were then analyzed on a FEI Nova600 FEG-SEM equipped with an EDAX EBSD detector. The EBSD maps generated were then imported in OIM analysis software for data presentation and post-analysis.

2.3. Sample preparation for TEM analysis

To prepare samples for TEM analysis, a cross section of the sample along the length of the wire was cut. Same sample preparation method as described above was used to polish the samples. A FEI Helios Nanolab 660 dual beam Focused Ion Beam (FIB) was used to lift-out an electron transparent lamella of the sample. To do this, a protective platinum layer was deposited on the region of interest. Two trenches were milled on either side of the region of interest. The lamella (or region of interest) was then welded to a needle and separated from the bulk material. The lamella was transferred onto a copper half grid and further thinning was performed at low beam current. The prepared

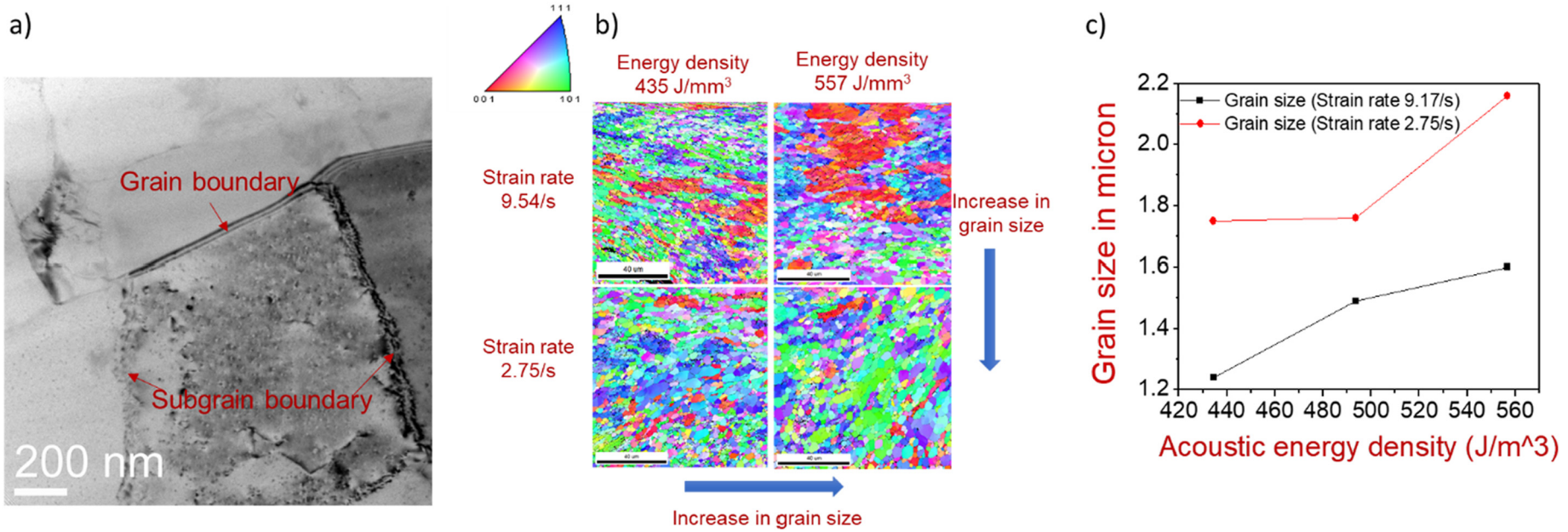

Fig. 1. a) Bright field TEM image of the after-deformation microstructure of pure aluminum wire compressed under simultaneous application of acoustic energy. b) EBSD micrographs of aluminum wires deformed under the presence of different ultrasonic energy densities and strain rates. c) Summary of the effect of ultrasonic energy density and strain rate on the grain size.

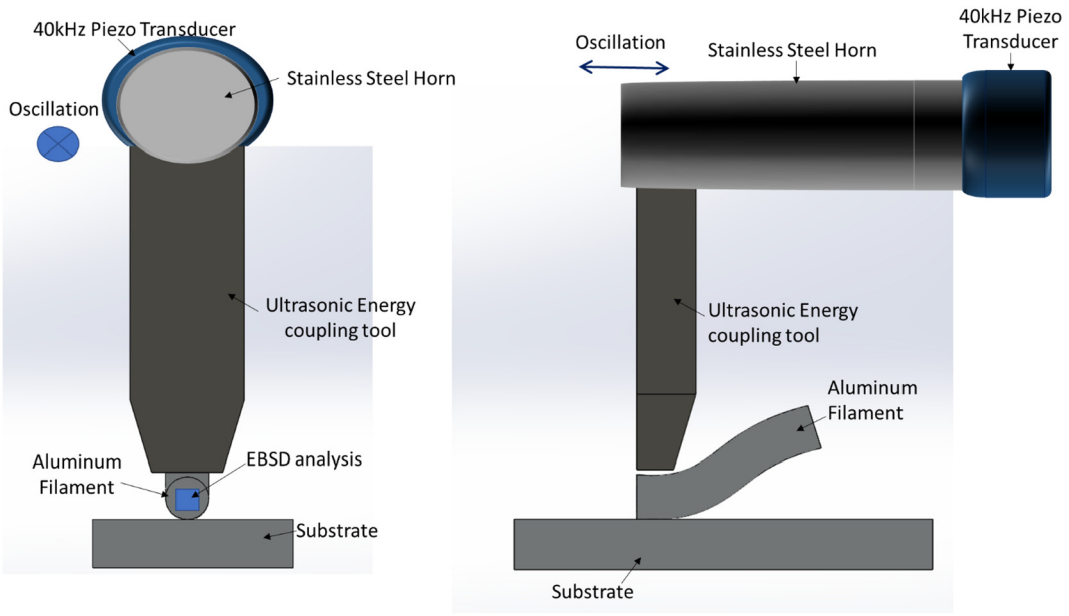

Fig. 2. Experimental setup for ultrasonic energy assisted compression testing of metal wires.

lamellas were analyzed in a 200 kV FEI Tecnai F20 TEM/STEM equipped with an EDAX EDS detector.

3. Results and discussion

3.1. Microstructure analysis of copper

Fig. 3 shows inverse pole figure (IPF) maps of undeformed copper wire, wire deformed without ultrasonic energy, and wire deformed with two different ultrasonic energy densities (500 J/m^3 and 710 J/m^3) and to a true strain of 0.51 and 0.75. Misorientations in the maps are with reference to the direction of compression, represented by the A1 axis. The average grain size of the undeformed wire is 3.68 μm with isotropic grains. The undeformed wire consists of annealing twins marked by red lines in Fig. 3a. After deformation, grains appear to be flattened and the grain size decreases to 0.89 μm for deformation without ultrasonic energy assistance. For deformation in the presence of ultrasonic energy, the average grain size is higher than that for deformation without ultrasonic energy. Also, the average grain size increases, albeit only slightly, with an increase in ultrasonic energy density applied during deformation. Fig. 3c and Fig. 3d show formation of small grains in the vicinity of grain boundaries of larger grains.

Fig. 4 shows the grain orientation spread map for the EBSD maps shown in Fig. 3. Grain orientation spread of each grain is calculated using the OIM software by first calculating the average orientation of the grain. Next, the misorientation of each pixel within the grain with respect to the average orientation of the entire grain is calculated. The average taken for all such misorientations within the grain determines the grain orientation spread of an individual grain. The formula used is given by $GOS(i) = \frac{1}{J(i)} \sum_j \omega_{ij}$, where $J(i)$ is the number of pixels in grain i, ω_{ij} is the misorientation angle between the orientation of pixel j and the average orientation of the grain i [28]. Typically, newly formed recrystallized grains have low deformation structure within them. Hence a low GOS value of 0–1.5 indicates a recrystallized grain, while values higher than 1.5 indicate deformed grains [28]. The undeformed wire has a high recrystallized grain fraction of 0.81 (Fig. 4a). This is attributed to the wire being annealed and having gone through static recrystallization process during annealing. As is evident from Fig. 4, there is an increase in the fraction of recrystallized grains (represented in blue colour) from 0.041 for deformation in absence of ultrasonic energy to ~0.068 for deformation in the presence of ultrasonic energy. With an increase in strain from 0.51 to 0.75, the fraction of recrystallized grains increases further to 0.125. The size of the recrystallized grains increases for deformation in presence of ultrasonic energy as well as upon increasing acoustic energy density during deformation.

TEM bright field images for copper sample deformed under the presence of ultrasonic energy (US energy density = 500 J/m^3) are shown in Fig. 5. The flattened substructure with a very high dislocation density in the interior is clearly evident from the Fig. 5a. Fig. 5b shows recrystallized grain in the substructure which has very different orientation as compared to the rest of the substructure evident by the contrast. The dislocation density in this grain is also relatively lower than that in the rest of the substructure. Fig. 5c shows formation of low angle subgrain boundaries in the vicinity of the grain boundary of the primary grain.

In warm and hot deformation of medium stacking fault energy materials such as copper, as explained in the Introduction section, the lack of dynamic recovery in the material leads to local increase in the dislocation density. Of particular interest is the region near the grain boundaries where the relatively large local misorientations give rise to formation of potential grain nucleation sites and eventual dynamic recrystallization of grains. A similar behavior can also be observed in ultrasonic energy assisted deformation. With further deformation accompanied by dislocation entanglement in regions similar to the ones shown in Fig. 5c, the local misorientation of these regions near the grain boundaries increases, leading to grain nucleation (grains depicted by blue colour in Fig. 4b, Fig. 4c and Fig. 4d).

For hot and warm deformation, it is well documented that the increase in deformation temperature or reduction in strain rate results in an increase in grain size and recrystallized grain volume fraction [26,29,30]. The grain size analysis shown in Fig. 3 indicates that when thermal energy is replaced with ultrasonic energy, analogous results in microstructure evolution can be observed. The increased fraction of recrystallized grains for deformation under the presence of ultrasonic energy can be attributed to the assistance of ultrasonic energy to formation of subgrain boundaries. This subgrain formation, particularly near the grain boundaries, results in the formation of regions with local misorientations and potential grain nucleation sites. An evidence of assistance to subgrain boundary (or low angle boundary) formation due to simultaneous application of ultrasonic energy can also be seen in Fig. 6b. It is worth noting that the area fraction of low angle boundaries

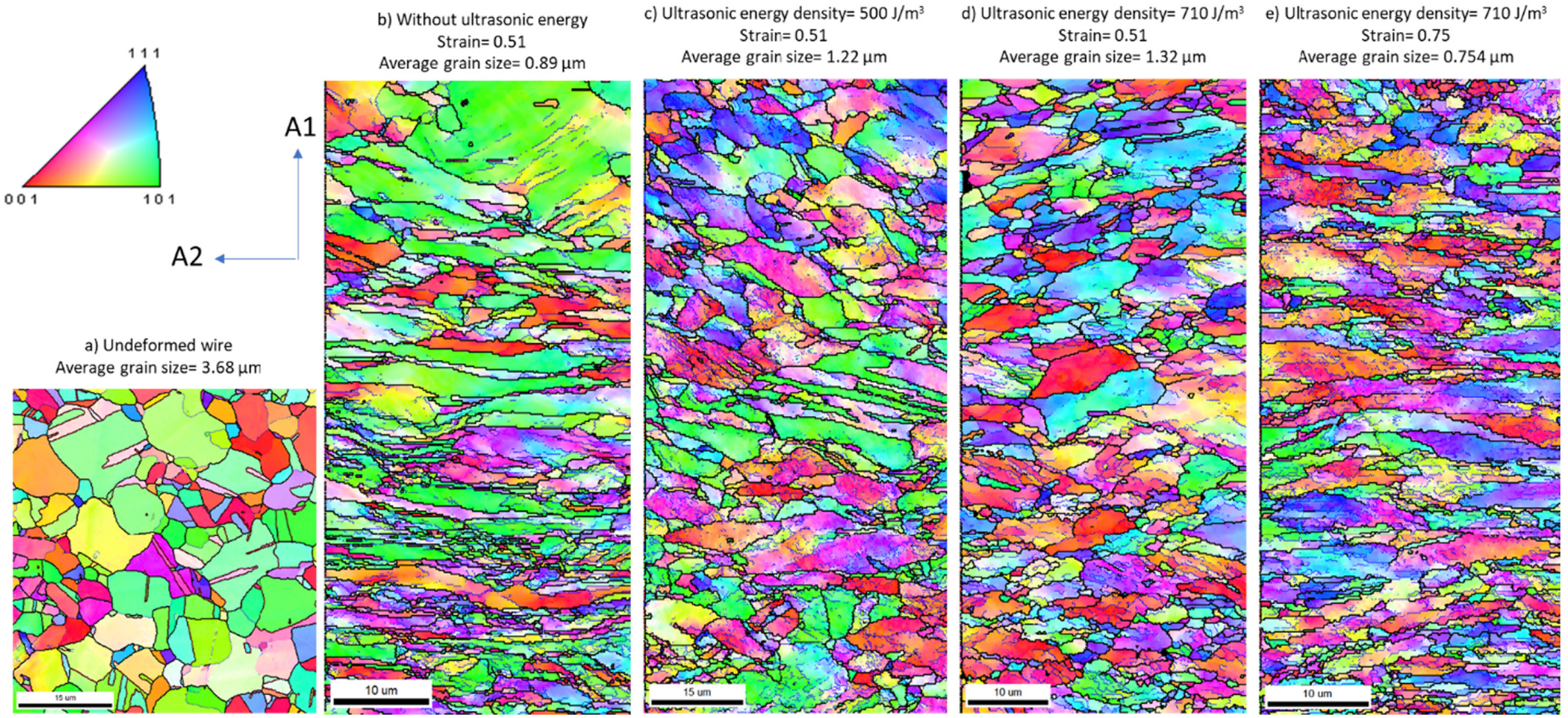

Fig. 3. EBSD map of a) Undeformed copper wire, b) copper wire deformed without any ultrasonic energy assistance, c) copper wire deformed with 500 J/m^3 ultrasonic energy density, copper wire deformed with 710 J/m^3 ultrasonic energy density and d) copper wire deformed with 710 J/m^3 ultrasonic energy density to a higher compressive strain of 0.75. High angle grain boundaries are highlighted by thick black lines while low angle grain boundaries (or subgrain boundaries) are highlighted by thin blue lines. A1 represents the direction of compression. (For interpretation of the references to colour in this figure legend, the reader is referred to the web version of this article.)

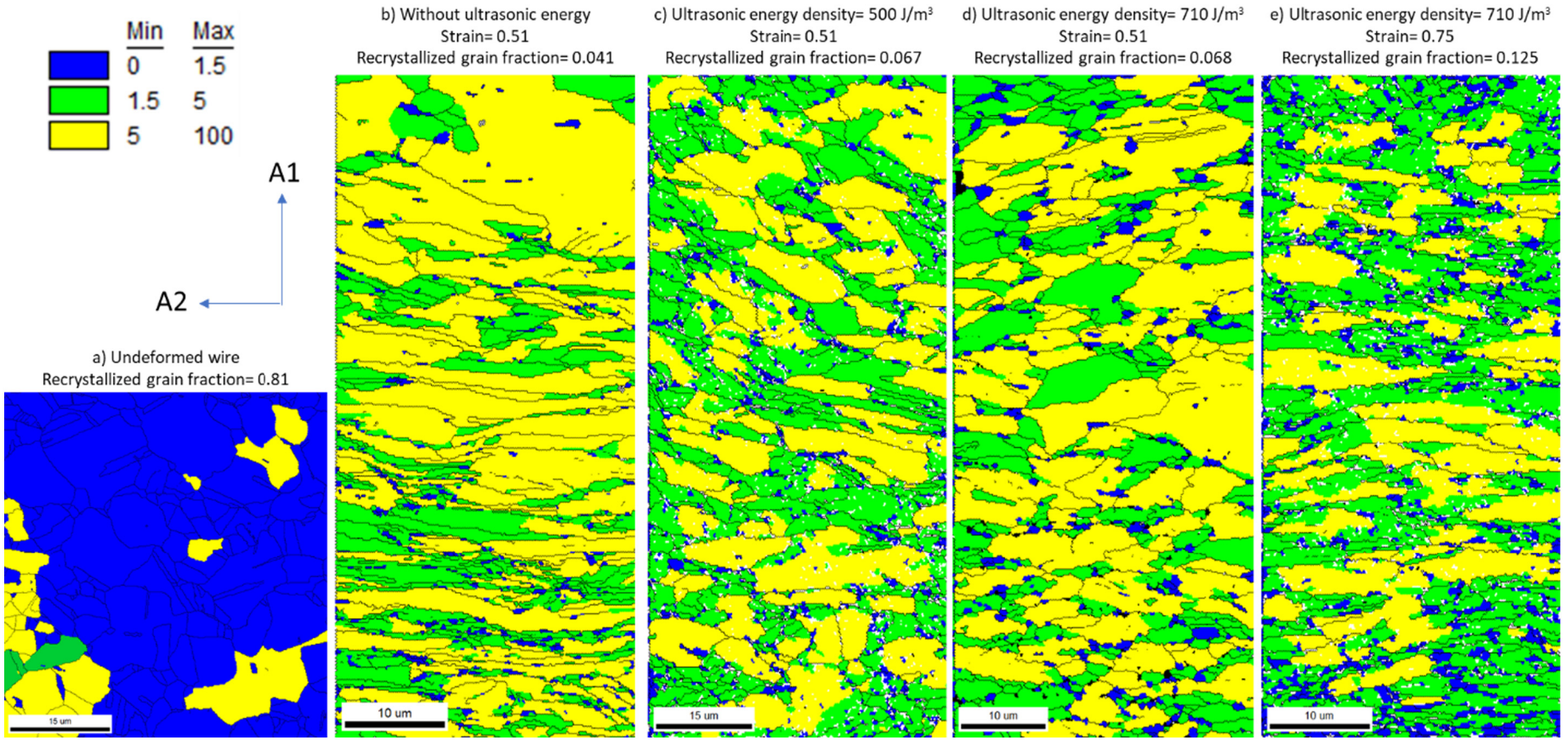

Fig. 4. Grain orientation spread (GOS) map of a) Undeformed copper wire, b) copper wire deformed without any ultrasonic energy assistance, c) copper wire deformed with 500 J/m^3 ultrasonic energy density, d) copper wire deformed with 710 J/m^3 ultrasonic energy density and e) copper wire deformed with 710 J/m^3 ultrasonic energy density to a higher compressive strain of 0.75. The blue grains have average GOS between 0 and 1.5, green ones have average GOS between 1.5 and 5 and yellow ones have average GOS between 5 and 100. (For interpretation of the references to colour in this figure legend, the reader is referred to the web version of this article.)

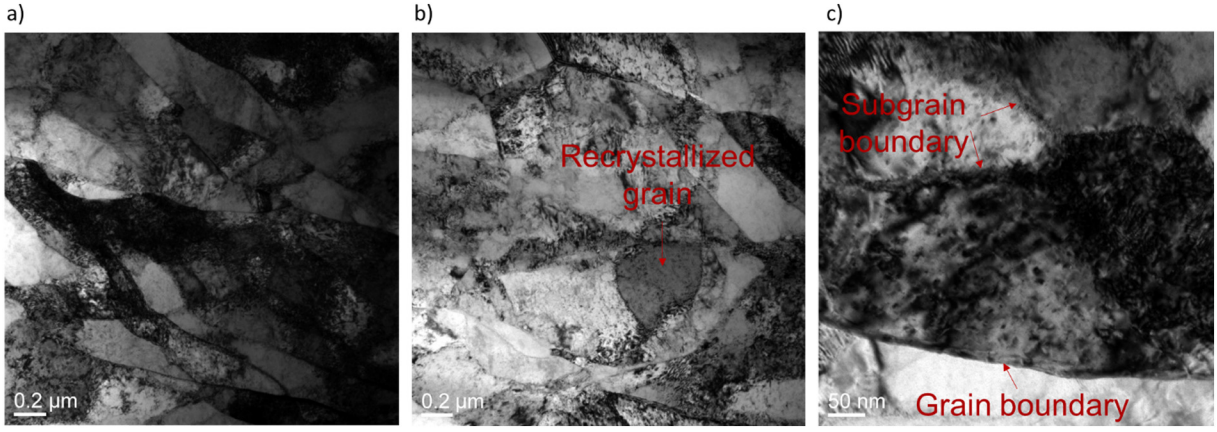

Fig. 5. TEM bright field images of copper sample after deformation under simultaneous application of ultrasonic energy (US energy density = 500 J/m^3. a) Flattened grain structure after deformation, b) Recrystallized grain marked by red arrow and c) Subgrain boundaries formed in the vicinity of a primary grain boundary. (For interpretation of the references to colour in this figure legend, the reader is referred to the web version of this article.)

(first 2 columns of the histogram) for copper samples deformed with ultrasonic energy (area fraction ≈ 0.4) is significantly higher than the area fraction for copper samples deformed without ultrasonic energy (area fraction ≈ 0.19). Similar assistance to subgrain formation was observed during ultrasonic energy assisted indentation experiments by Siu et al. [31].

The complete absence of such recrystallization in aluminum after ultrasonic energy assisted deformation, as seen in Fig. 1 and [24], is because aluminum has high stacking fault energy. This promotes dynamic recovery during deformation of aluminum assisted by ultrasonic energy. Hence, despite the presence of formation of low angle or subgrain boundaries (as seen in Fig. 1a), the low dislocation density prevents local misorientations from increasing, thereby suppressing DDRX. The very high fraction of low angle boundaries in copper as compared to aluminum, as is evident from Fig. 6a, also indicates higher local misorientations within the primary grains, which contribute to increased DDRX. Even though aluminum and copper have the same FCC crystal structure, it is the difference in their stacking fault energies that in fact, results in a markedly different microstructure after deformation in the presence of ultrasonic energy.

3.2. Microstructure analysis of Al6061

Fig. 7 shows the inverse pole figure maps for undeformed Al6061 wire and wires deformed to a true strain of 0.75 under the presence of ultrasonic energy density of 150 J/m^3 and 215 J/m^3. As noted in the earlier case, misorientations in the maps are with reference to the direction of compression, represented by the A1 axis. The microstructure of the undeformed wire shows annealed grain structure with an average grain size of 6.05 μm. The map shows negligible amount of subgrain boundaries. In contrast, the EBSD map of wires deformed under the presence of ultrasonic energy show substantial subgrain formation. The after-deformation grain size decreases, and very fine grains appear at the grain boundaries of larger grains. For deformation using ultrasonic energy density of 150 J/m^3, the average grain size is 0.33 μm while it increases to 0.52 μm in the case of using ultrasonic energy density of 215 J/m^3.

The corresponding grain orientation spread maps of the EBSD maps in Fig. 7 are shown in Fig. 8. The undeformed wire has a high recrystallized grain fraction of 0.87 since it has gone through static recrystallization during heat treatment. A very high fraction of recrystallized grains (~0.36), depicted by blue colour, can be seen in the

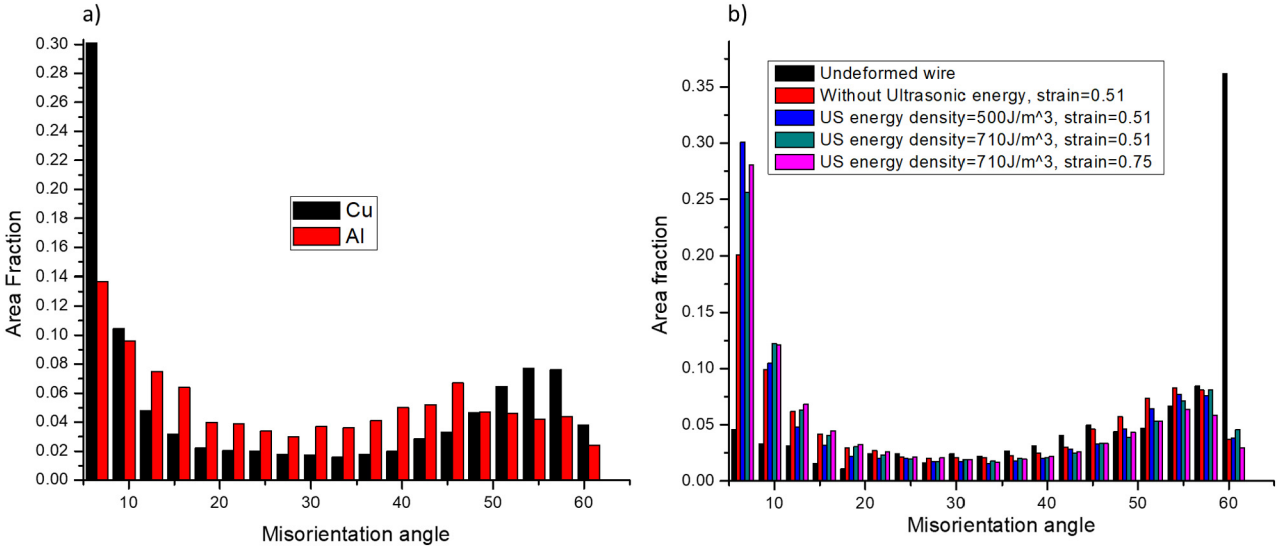

Fig. 6. Misorientation angle versus area fraction histogram for- a) Copper and aluminum deformed under the presence of same ultrasonic energy density and b) undeformed copper wire, copper deformed without ultrasonic energy, copper deformed in the presence of ultrasonic energy density of 500 J/m^3, 710 J/m^3 and copper deformed in the presence of ultrasonic energy density of 710 J/m^3 to a higher strain.

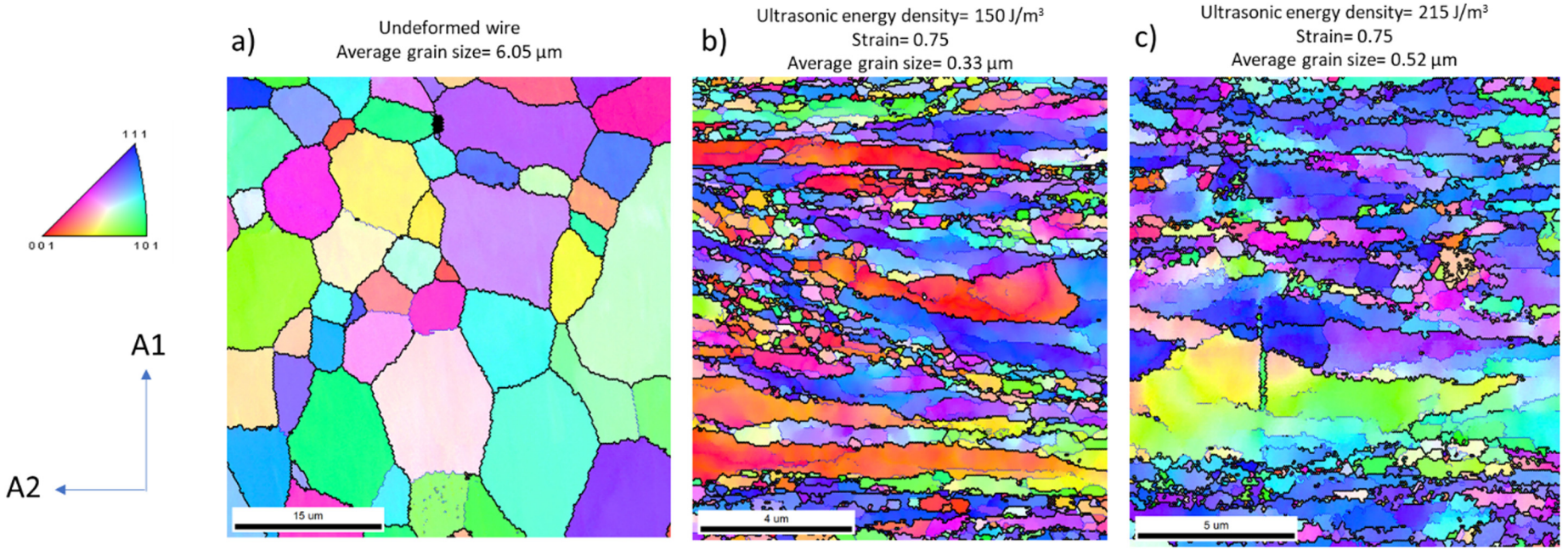

Fig. 7. Inverse pole figure maps of a) Undeformed Al6061 wires, b) Al6061 wire deformed under the presence of ultrasonic energy density of 150 J/m^3 and c) Al6061 wire deformed under the presence of ultrasonic energy density of 215 J/m^3, b) and c) both compressed to a strain of 0.75. High angle grain boundaries are highlighted by thick black lines while low angle grain boundaries (or subgrain boundaries) are highlighted by thin blue lines. A1 represents the direction of compression. (For interpretation of the references to colour in this figure legend, the reader is referred to the web version of this article.)

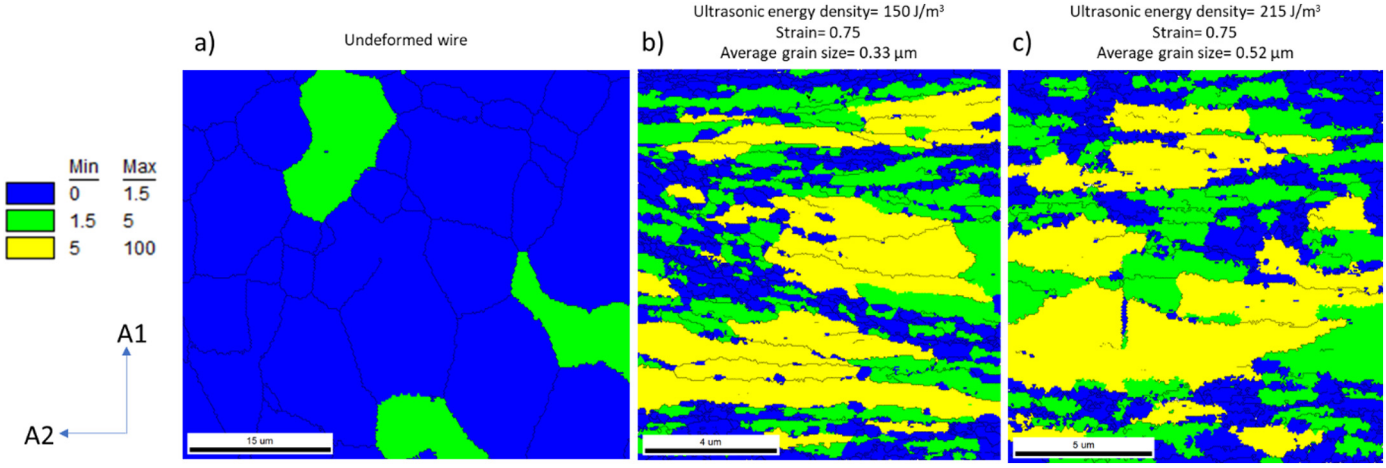

Fig. 8. Grain orientation spread (GOS) map of- a) undeformed Al6061 wire, b) Al6061 wire deformed with 150 J/m^3 ultrasonic energy density and c) Al6061 wire deformed with 215 J/m^3. The blue grains have average GOS between 0 and 1.5, green ones have average GOS between 1.5 and 5 and yellow ones have average GOS between 5 and 100. (For interpretation of the references to colour in this figure legend, the reader is referred to the web version of this article.)

GOS maps. The comparison of overall average of such maps revealed no significant change in the fraction of recrystallized grains upon varying ultrasonic energy density.

The STEM image in Fig. 9a shows a classical recrystallization microstructure with a larger grain surrounded by smaller recrystallized grains. Al6061 alloy is a precipitation hardened Al-Mg-Si alloy. The Mg_2Si precipitates in the alloy provide hindrance to dislocation motion [32]. These precipitates are shown in Fig. 9b, marked by red arrows. An EDS map of the sample shown in Fig. 10 illustrates the elemental distribution in the precipitates and the matrix. It can be seen that Si, Cr and Fe are concentrated in the precipitates while Mg and Cu are distributed uniformly. Some precipitates are richer in Cr and Fe as seen from the two tables listing the quantitative EDS analysis in the respective precipitates shown in the electron image (precipitate 2 is richer than precipitate 1). In Fig. 9c, a subgrain boundary formed by entangled dislocations (marked by red arrow) can be seen along with other dislocations within the subgrain. The overall dislocation density is much lower than that observed for copper samples.

The grain refinement observed in the post-deformation microstructure of samples deformed under simultaneous application of ultrasonic energy (Fig. 7) can be attributed to the recrystallization, as observed in Fig. 8. Although aluminum alloys have a high stacking fault energy, these alloys have shown to undergo recrystallization during hot deformation. The recrystallization is primarily caused by formation of serrated grain boundaries which get pinched during deformation. The pinching results in formation of small grains of the order of subgrains at the boundaries of larger grains. This phenomenon called geometric dynamic recrystallization (gDRX) has been observed for aluminum alloys [27,33,34].

As argued before, recrystallization was not observed in Aluminum under similar conditions of ultrasonic energy and strain rate (Fig. 1 and [24]). There are two possible explanations for observation of gDRX in Al6061 and not in pure aluminum. Al6061 alloys contain precipitates which obstruct dislocation motion. This in turn causes the occurrence of dislocation pile-up and generation of new dislocations at the precipitates, as shown in Fig. 9b and Fig. 9c. Interaction of local dislocations with pile-ups results in subsequent formation of subgrains, which in fact are the cause for formation of serrated grain boundaries [34]. The second factor is that the initial average grain size of the undeformed pure aluminum wire was ~10 µm while the average size of the undeformed Al6061 wire was ~6 µm. It has been observed during hot deformation process that the reduction in initial grain size facilitate the initiation of gDRX at a lower value of strain [27]. During compression, the width (i.e. dimension along the compression direction) of grains with smaller initial size approaches the subgrain size at a lower strain value. Hence, the pinching-off of subgrains and subsequent gDRX happens at a lower strain value than that for grains with larger initial size. Hence, the smaller grain size of Al6061 wire definitely contributed to the observation of gDRX in Al6061. However, whether it was the only factor or whether the precipitates in Al6061 also played a role in

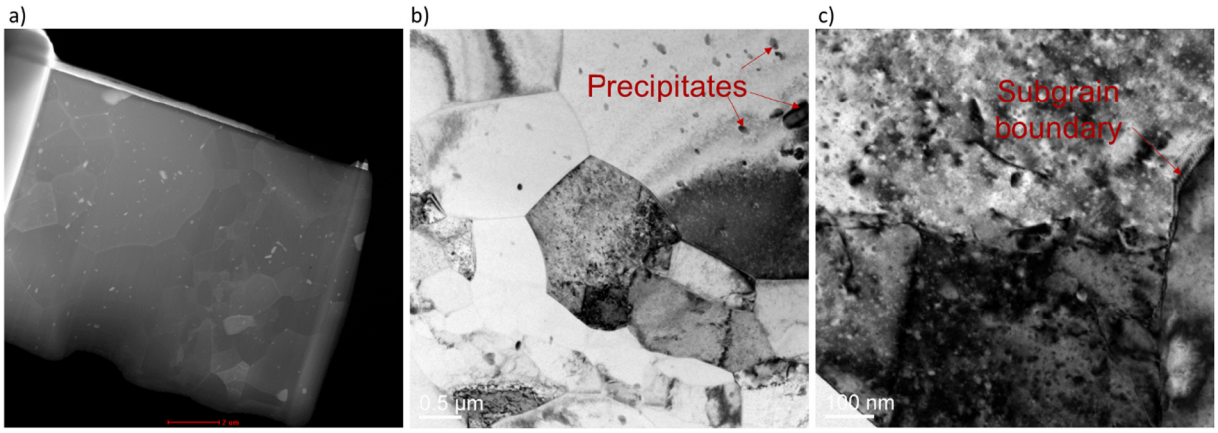

Fig. 9. a) STEM image of Al6061 wire deformed with 210 J/m^3 ultrasonic energy density, b) bright field TEM image of the same sample showing precipitates and, c) bright field TEM image showing subgrain boundary.

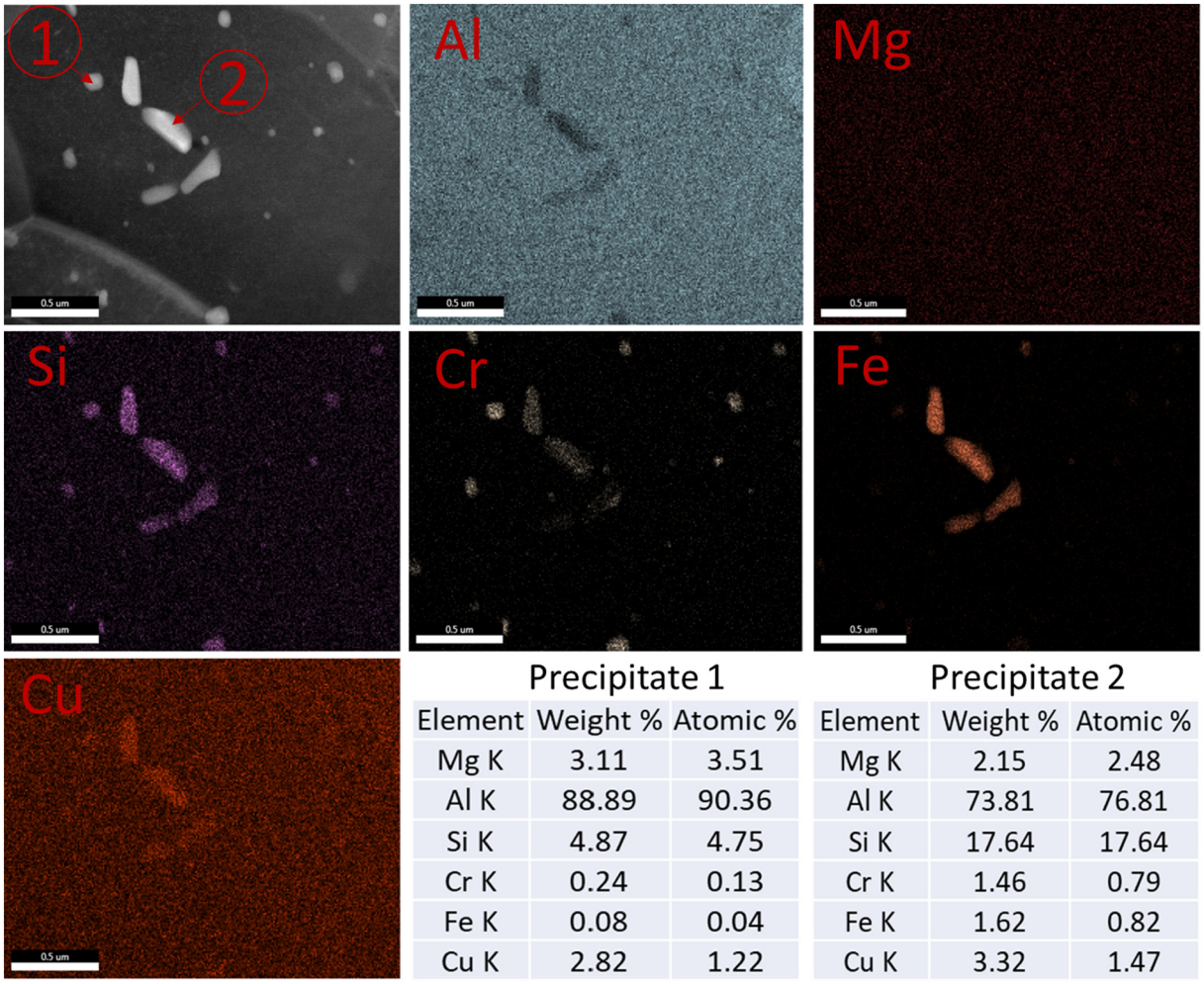

Precipitate 1

Element	Weight %	Atomic %
Mg K	3.11	3.51
Al K	88.89	90.36
Si K	4.87	4.75
Cr K	0.24	0.13
Fe K	0.08	0.04
Cu K	2.82	1.22

Precipitate 2

Element	Weight %	Atomic %
Mg K	2.15	2.48
Al K	73.81	76.81
Si K	17.64	17.64
Cr K	1.46	0.79
Fe K	1.62	0.82
Cu K	3.32	1.47

Fig. 10. EDS map of the Al6061 sample deformed with 210 J/m^3 ultrasonic energy density. Tables show the quantitative EDS point analysis for the 2 precipitates shown in the electron image.

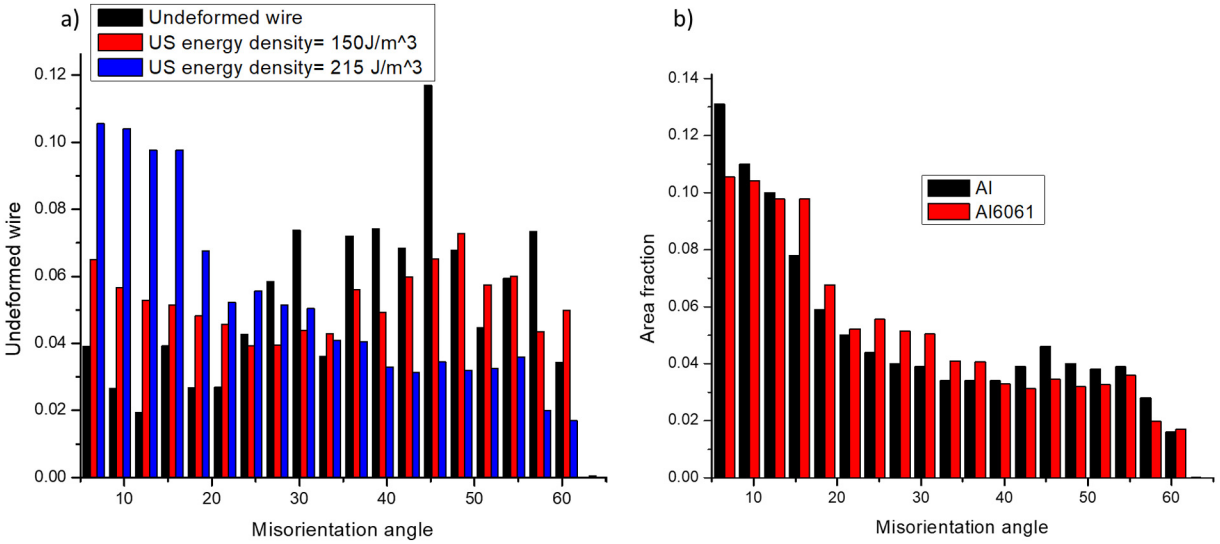

Fig. 11. Misorientation angle versus area fraction histogram for - a) undeformed Al6061 wire, Al6061 wire deformed under ultrasonic energy density of 150 J/m^3 and 215 J/m^3, b) Aluminum and Al6061 deformed under similar conditions of ultrasonic energy density.

this process requires further investigation.

The assistance to subgrain formation due to simultaneous application of ultrasonic energy is evident from the misorientation angle versus area fraction graph shown in Fig. 11a. The fraction of subgrain boundaries or low angle boundaries (first 2 columns in the histogram) significantly increases upon an increase in ultrasonic energy density. The average grain size and the size of the grains which have gone through gDRX depend on the subgrain size [27]. It was observed in [24] that for pure aluminum, the subgrain size increases with an increase in ultrasonic energy density due to coarsening of subgrain network caused by assistance of ultrasonic energy to dislocation annihilation. For Al6061, the increase in average grain size and the size of recrystallized grains (Fig. 7) with an increase in ultrasonic energy density can be attributed to this increase in subgrain size. The lesser fraction of subgrain boundaries for Al6061 as compared to pure aluminum, as evident from Fig. 11b, is due to gDRX of subgrains which transforms subgrain boundaries into high angle boundaries.

4. Conclusion

In this work, a detailed analysis of the effect of stacking fault energy on the microstructure of FCC metals during ultrasonic energy assisted deformation was conducted. It was observed that ultrasonic energy assists in subgrain formation, which is in line with earlier observations made in the literature [31]. A comparison of microstructure of medium stacking fault energy metal (copper) and high stacking fault energy metal (aluminum from previous studies) was made using EBSD and TEM analysis. For copper, which is a medium stacking fault energy metal, lack of dynamic recovery resulted in high dislocation density. Grain spread orientation maps provided evidence of discontinuous dynamic recrystallization (DDRX) similar to that observed in hot deformation. For Al6061 however, geometric dynamic recrystallization (gDRX) caused by pinching-off of serrated grain boundaries was observed after ultrasonic energy assisted deformation. The microstructure evolution of copper and Al6061 was found to be very different from that of pure Al, in which dynamic recovery was found to be the dominant mechanism. The insights reported here improve upon the current understanding of the effect of ultrasonic energy irradiation during deformation on the microstructure of FCC metals.

Data availability statement

The raw/processed data required to reproduce these findings cannot be shared at this time as the data also forms part of an ongoing study.

References

[1] B. Langenecker, Effects of ultrasound on deformation characteristics, IEEE Trans. Sonics Ultrasonics SU-13 (1) (March 1966).

[2] C. Yang, X. Shan, T. Xie, Titanium wire drawing with longitudinal-torsional composite ultrasonic vibration, Int. J. Adv. Manuf. Technol. 83 (2016) 645–655.

[3] S. Amini, A.H. Gollo, H. Paktinat, An investigation of conventional and ultrasonic-assisted forming of annealed AA1050 sheet, Int. J. Adv. Manuf. Technol. 90 (5—8) (2016) 1569–1578.

[4] A. Abdullah, M. Paknejad, S. Dashti, A. Pak, A.M. Beigi, Theoretical and experimental analyses of ultrasonic-assisted indentation forming of tube, J. Eng. Manuf. 228 (3) (2014) 388–398.

[5] Y.B. Zhong, C.S. Wu, G.K. Padhy, Effect of ultrasonic vibration on welding load, temperature and material flow in friction stir welding, J. Mater. Process. Technol. 239 (2017) 273–283.

[6] J.A. George, G. Harman, The ultrasonic welding mechanism as applied to aluminum- and gold-wire bonding in microelectronics, IEEE Transaction on parts PHP-13 (1) (December 1977).

[7] W. F., L. H., J. Z., Junhui Li, Theoretical and experimental analyses of atom diffusion characteristics on wire bonding, J. Phys. D. Appl. Phys. 41 (2008).

[8] M. L., J.-M. K., D.-W. K., C. W., Hongjun Ji, Nano features of Al/Au ultrasonic bond interface observed by high resolution transmission electron microscopy, Mater. Charact. 59 (2008) 1419–1424.

[9] E. Mariani, E. Ghassemieh, Microstructure evolution of 6061 O Al alloy during ultrasonic consolidation: an insight form electron backscatter diffraction, Acta Mater. 58 (2009) 2492–2503.

[10] J. Sietins, J. Gillespie, S. Advani, Transmission electron microscopy of an ultrasonically consolidated copper-aluminum interface, J. Mater. Res. 29 (17) (2014) 1970–1977.

[11] J. W. G. J., S. G. A., T. A. B. Steve Koellhoffer, "Role of friction on the thermal development in ultrasonically consolidated aluminum foils and composites," J. Mater. Process. Technol., vol. 211, no. 11, pp. 1864–1877, November 2011.

[12] A. Macwan, D.L. Chen, Microstructure and mechanical properties of ultrasonic spot welded copper-to-magnesium alloy joints, Mater. Des. 84 (2015) 261–269.

[13] C.Q. Zhang, J.D. Robson, O. Ciuca, P.B. Prangnell, Microstructural characterization and mechanical properties of high power ultrasonic spot welded aluminum alloy AA6111-Ti-Al6V4 dissimilar joints, Mater. Charact. 97 (2014) 83–91.

[14] H. Peng, D. Chen, X. Jiang, Microstructure and mechanical properties of an ultrasonic spot welded aluminum alloy: the effect of welding energy, Materials 10 (2017) 449–464.

[15] G. Liu, X. Hu, Y. Fu, Y. Li, Microstructure and mechanical properties of ultrasonic welded joint of 1060 aluminum alloy and T2 pure copper, Metals 7 (2017) 361–371.

[16] A. Deshpande, K. Hsu, Acoustoplastic metal direct-write: towards solid aluminum 3D printing in ambient conditions, Addit. Manuf. 19 (2018) 73–80.

[17] A. Rusinko, Analytical description of ultrasonic hardening and softening, Ultrasonics 51 (2011) 709–714.

[18] E.G. Amir Siddiq, Thermomechanical analyses of ultrasonic welding process using, Mech. Mater. 40 (2008) 982–1000.

[19] G.-Y. K., Z. W., L. F., Q. Z., D. M., Z. C., Zhehe Yao, "Acoustic softening and residual hardening in aluminum: modeling," Int. J. Plast., vol. 39, pp. 75–87, 2012.

[20] Z. Zhu, B.P. Wynne, E. Ghassemieh, A. Siddiq, Microstructural analysis of ultrasonic welded AA6061 by electron backscattered diffraction, Rare Metal Mater. Eng. 28 (3) (2009) 147–151.

[21] A. Siddiq, T. El Sayed, A thermomechanical crystal plasticity constitutive model for ultrasonic consolidation, Comput. Mater. Sci. 51 (1) (2012) 241–251.

[22] A. Siddiq, T. El Sayed, Acoustic softening in metals during ultrasonic assisted deformation via CP-FEM, Mater. Lett. 65 (2) (2011) 356–359.

[23] H. Zhou, H. Cui, Q.-H. Qin, H. Wang, Y. Shen, A comparative study of mechanical and microstructural characteristics of aluminium and titanium undergoing ultrasonic assisted compression testing, Mater. Sci. Eng. A 682 (2017) 376–388.

[24] A. Deshpande, K. Hsu, Acoustic energy enabled dynamic recovery in aluminium and its effects on stress evolution and post-deformation microstructure, Mater. Sci. Eng. A 711 (2018) 62–68.

[25] T. Sakai, A. Belyakov, R. Kaibyshev, H. Miura, J.J. Jonas, Dynamic and post-dynamic recrystallization under hot, cold and severe plastic deformation conditions, Prog. Mater. Sci. 60 (2013) 130–207 October.

[26] K. Huang, R.E. Loge, A review of dynamic recrystallization ohenomena in metallic materials, Mater. Des. 111 (2016) 548–574.

[27] W. Blum, Q. Zhu, R. Merkel, H.J. McQueen, Geometric dynamic recrystallization in hot torsion of Al-5Mg-0.6Mn, Mater. Sci. Eng. A 205 (1996) 23–30.

[28] A. Hadadzadeh, F. Mokdad, M.A. Wells, D.L. Chen, A new grain orientation spread approach to analyze the dynamic recrystallization behavior of a cast-homoginized Mg-Zn-Zr alloy using electron backscatter diffraction, Mater. Sci. Eng. A 709 (2018) 285–289.

[29] A.M. Wusatowska-Sarnek, The new grain formation during warm and hot deformation of copper, J. Eng. Mater. Technol. 127 (2005) 295–300.

[30] H.J. McQueen, C.A.C. Imbert, Dynamic recrystallisation: plasticity enhancing structural development, J. Alloys Compd. 378 (2004) 35–43.

[31] K.W. Siu, A.H.W. Ngan, I.P. Jones, New insight on acoustoplasticity – ultrasonic irradiation enhances subgrain formation during deformation, Int. J. Plast. 27 (2011) 788–800.

[32] H.J. McQueen, S. Spigarelli, M.E. Kassner, E. Evangelista, Hot Deformation and Processing of Aluminum Alloys, CRC press, 2011.

[33] W.H. Van Geertruyden, W.Z. Misiolek, P.T. Wang, Grain structure in a 6061 aluminum alloy during torsion, Mater. Sci. Eng. A 419 (2006) 105–114.

[34] H.J. McQueen, I. Poschmann, Subgrain development in hot working of Al and Al-5Mg, Mater. Sci. Eng. A (1997) 830–833, 1997.